





Geophysical Research Letters[®]



RESEARCH LETTER

10.1029/2022GL101628

Inter-Calibration of Geostationary Imager Infrared Bands Using a Hyperspectral Sounder on the Same Platform

Di Di^{1,2} , Yue Liu³, Jun Li⁴ , Ronglian Zhou⁵, Zhenglong Li⁶ , and Xinya Gong⁴ 

Key Points:

- Geostationary (GEO) hyperspectral IR sounder has the unique advantage to inter-calibrate GEO imager infrared (IR) bands at the same observation time and geometry
- Geostationary Interferometric Infrared Sounder /Advanced Geosynchronous Radiation Imager differences indicate less viewing angle dependence but significant diurnal variations
- The GEO-GEO inter-comparisons benefit quantitative applications of GEO imager measurements

Supporting Information:

Supporting Information may be found in the online version of this article.

Correspondence to:

J. Li,
junli@cma.gov.cn

Citation:

Di, D., Liu, Y., Li, J., Zhou, R., Li, Z., & Gong, X. (2023). Inter-calibration of geostationary imager infrared bands using a hyperspectral sounder on the same platform. *Geophysical Research Letters*, 50, e2022GL101628. <https://doi.org/10.1029/2022GL101628>

Received 19 OCT 2022

Accepted 21 JAN 2023

Author Contributions:

Conceptualization: Jun Li
Data curation: Yue Liu, Ronglian Zhou
Formal analysis: Zhenglong Li
Funding acquisition: Jun Li
Investigation: Di Di, Ronglian Zhou
Methodology: Di Di
Project Administration: Jun Li
Resources: Ronglian Zhou
Software: Di Di, Yue Liu
Supervision: Jun Li
Validation: Zhenglong Li, Xinya Gong
Visualization: Yue Liu

¹Collaborative Innovation Center on Forecast and Evaluation of Meteorological Disasters, Nanjing University of Information Science and Technology, Nanjing, China, ²Key Laboratory for Aerosol-Cloud-Precipitation, School of Atmospheric Physics, China Meteorological Administration, Nanjing University of Information Science and Technology, Nanjing, China, ³School of Atmospheric Science, Nanjing University of Information Science and Technology, Nanjing, China, ⁴FYSIC, National Satellite Meteorological Center, China Meteorological Administration, Beijing, China, ⁵Chinese Academy of Meteorological Sciences, China Meteorological Administration, Beijing, China, ⁶Cooperative Institute for Meteorological Satellite Studies, University of Wisconsin-Madison, Madison, WI, USA

Abstract Geostationary (GEO) imager Infrared (IR) bands are often intercalibrated with hyperspectral IR sounders onboard low earth orbit (LEO) satellites. Due to viewing geometry and time differences between GEO and LEO, the inter-calibration is limited to certain viewing angles and times. When a GEO hyperspectral IR sounder and GEO imager are on the same platform, the inter-calibration can be conducted from all angles and at all times. In this study, the Geostationary Interferometric Infrared Sounder (GIIRS) is used to inter-calibrate the Advanced Geosynchronous Radiation Imager (AGRI), both onboard FengYun-4A. Radiance inter-comparisons between GIIRS and AGRI under homogeneous scenes, including both clear and cloudy situations, indicate that the differences are within 1 K. The differences have obvious dependence on scene radiance, less dependence on the cloudy situation, and the local zenith angle when it is less than 70°. However, they exhibit significant diurnal characteristics.

Plain Language Summary Inter-calibration is an important way to monitor, improve and harmonize the quality of observations from operational weather and environmental satellites. It aims to ensure consistent accuracy among space-based observations worldwide for climate monitoring, weather forecasting, and environmental applications. Usually, geostationary (GEO) imager infrared (IR) bands are inter-calibrated with a hyperspectral IR sounder onboard a low earth orbit (LEO) satellite. Due to viewing geometry differences between GEO and LEO, the inter-calibration is limited to certain viewing angles and LEO overpass times. When a GEO hyperspectral IR sounder and GEO imager are on the same platform, the inter-calibration is more accurate, and the calibration bias can be well understood for applications. In particular, the angle and scene dependence, and the diurnal characteristics of GEO imager radiance observations can be well quantified. This study analyzes GEO imager IR band calibration bias characteristics when the hyperspectral IR sounder is on the same platform. Because GEO hyperspectral IR sounders have been developed in China and are being planned in Europe, U.S., and Japan, this study provides scientific evidence of the importance of placing an advanced imager and sounder together in the same GEO orbit.

1. Introduction

Using meteorological satellites for long-term and continuous observations plays an important role in weather, climate, and environmental research. Due to the degradation of satellite sensors, performance stability needs to be monitored and evaluated and corrected for any degradation. Imagers onboard geostationary (GEO) weather satellites are important sensors for observing the environment and weather with both high temporal and spatial resolutions.

Inter-calibration based on a hyperspectral sensor with high calibration accuracy is an effective way to evaluate the in-orbit calibration accuracy of a broad band imager (Hewison et al., 2013). The existing polar-orbiting hyperspectral IR sensors, such as Infrared Atmospheric Sounder Interferometer (IASI), Cross-track Infrared Sounder (CrIS), and Atmospheric Infrared Sounder (AIRS) (Menzel et al., 2018) have high radiometric/spectral calibration accuracy with stability in-orbit (Aumann et al., 2006; Blumstein et al., 2007; Taylor et al., 2015; Wang et al., 2011). They have been well-calibrated pre-launch and post-launch and are often used as benchmark instruments to evaluate the IR band calibration accuracy of broad band imagers (Wang et al., 2009; Wu

© 2023. The Authors.

This is an open access article under the terms of the [Creative Commons Attribution-NonCommercial-NoDerivs License](https://creativecommons.org/licenses/by/4.0/), which permits use and distribution in any medium, provided the original work is properly cited, the use is non-commercial and no modifications or adaptations are made.

Writing – original draft: Di Di
Writing – review & editing: Jun Li,
Zhenglong Li

et al., 2009). In general, imagers onboard polar orbiting satellites, such as the MODerate resolution Imaging Spectroradiometer (MODIS), Visible Infrared Imaging Radiometer Suite (VIIRS), Advanced Very High Resolution Radiometer (AVHRR), etc., can be inter-calibrated with a hyperspectral IR sounder onboard the same platform (Gong et al., 2018; Moeller et al., 2013), while GEO imagers can also be inter-calibrated with collocated hyperspectral IR sounders from low earth orbit (LEO) satellites (He et al., 2022; Hewison et al., 2013; Hu et al., 2013; Wang et al., 2009), which is useful for monitoring the stability of the imagers' IR band calibration accuracy.

In principle, the collocated observations from the monitored and reference instruments should cover all scenes, which enables users to identify any observation bias with possible scene dependence. However, due to viewing geometry differences between GEO and LEO, the inter-calibration is limited to certain angles and overpass times. Furthermore, these differences can introduce uncertainty to the inter-calibration results, meaning the uncertainty in differences between a GEO imager and a LEO sounder is larger than that if the imager is on the same LEO platform. When the hyperspectral IR sounder is on the same GEO platform, the GEO imager IR bands can be intercalibrated with much greater spatial coverage over different scenes. In addition, the temporal characteristics of the brightness temperature (BT) differences (BTD) between imager and sounder can be well captured and understood, which is very useful for quantitative applications of GEO imager observations. For example, understanding the GEO imager calibration diurnal bias is very useful for assimilating radiances into numerical weather prediction (NWP) models. Furthermore, understanding the imager calibration uncertainty characteristics is also very important for improving the operational products for better applications. Therefore, it is important to address inter-calibration science questions related to the situation where both the imager and the sounder are on the same platform. Such questions include: how to analyze the imager calibration uncertainties for all angles, all scenes, large coverage, and all times? And for a given imager sensor, what are the calibration uncertainty characteristics, especially the diurnal characteristics?

The Geostationary Interferometric Infrared Sounder (GIIRS) onboard FengYun-4A is the first hyperspectral IR sounder in a GEO orbit. Inter-comparisons were made using observations from IASI, an excellent inter-calibration reference with a radiometric sensitivity of 0.1–0.5 K which is consistent with AIRS on the Aqua satellite with uncertainties around 0.1 K (Blumstein et al., 2007; He et al., 2022; Wang et al., 2011). These analyses from a 7-day period using the simultaneous nadir overpass (SNO) method indicate that most atmospheric absorption lines of GIIRS in the long-wave band closely coincide with those of IASI with good radiometric accuracy and spectral inconsistency less than 10 ppm (Guo et al., 2021). Therefore, the GIIRS can be used to inter-calibrate the Advanced Geosynchronous Radiation Imager (AGRI) on the same platform. Using GIIRS and AGRI from FengYun-4A (Yang et al., 2017), this study addresses GEO imager specific calibration questions such as viewing angle dependence, scene dependence (land/sea, clouds, etc), and diurnal characteristics.

Section 2 describes the data and method; Section 3 explains schemes for quality control (QC) and analyzes the angle dependence, scene radiance dependence, and diurnal characteristics; Summary and discussions are given in Section 4.

2. Data and Methodology

2.1. Instruments and Data

Similar to other advanced GEO imagers such as AHI (Bessho et al., 2016) and ABI (Schmit et al., 2005), the AGRI onboard FY-4A has 14 spectral bands with a spatial resolution of 0.5–4 km (0.5–1 km for visible band, 2 km for near-IR band, and 4 km for IR bands). AGRI also provides observations every 15 min with full disk coverage. In this study, the full disk Level 1B radiance data are used, and which means the GIIRS radiance measurements have been processed with geolocation, spectral, and radiometric calibration by the National Satellite Meteorological Center of China. In addition, the AGRI Level 2 cloud mask and cloud-top height (CTH) products are also used for determining the GIIRS sub-footprint homogeneity, especially the sub-footprint cloud situations within the GIIRS sub-field-of-view (FOV) or sub-footprint.

GIIRS observes top-of-atmosphere radiances with 689 channels (700–1,130 cm^{-1} or 8.85–14.29 μm) in the long-wave spectral region and 961 channels (1,650–2,250 cm^{-1} , or 4.44–6.06 μm) in the middle wave spectral region with a spectral resolution of 0.625 cm^{-1} which is similar to LEO hyperspectral IR sounders. GIIRS provides atmospheric vertical temperature and moisture information every 2 hr over China and its surrounding areas (3–55°N; 60–137°E). The spatial resolution is 16 km at nadir (note that it is 12 km for GIIRS onboard FY-4B). In

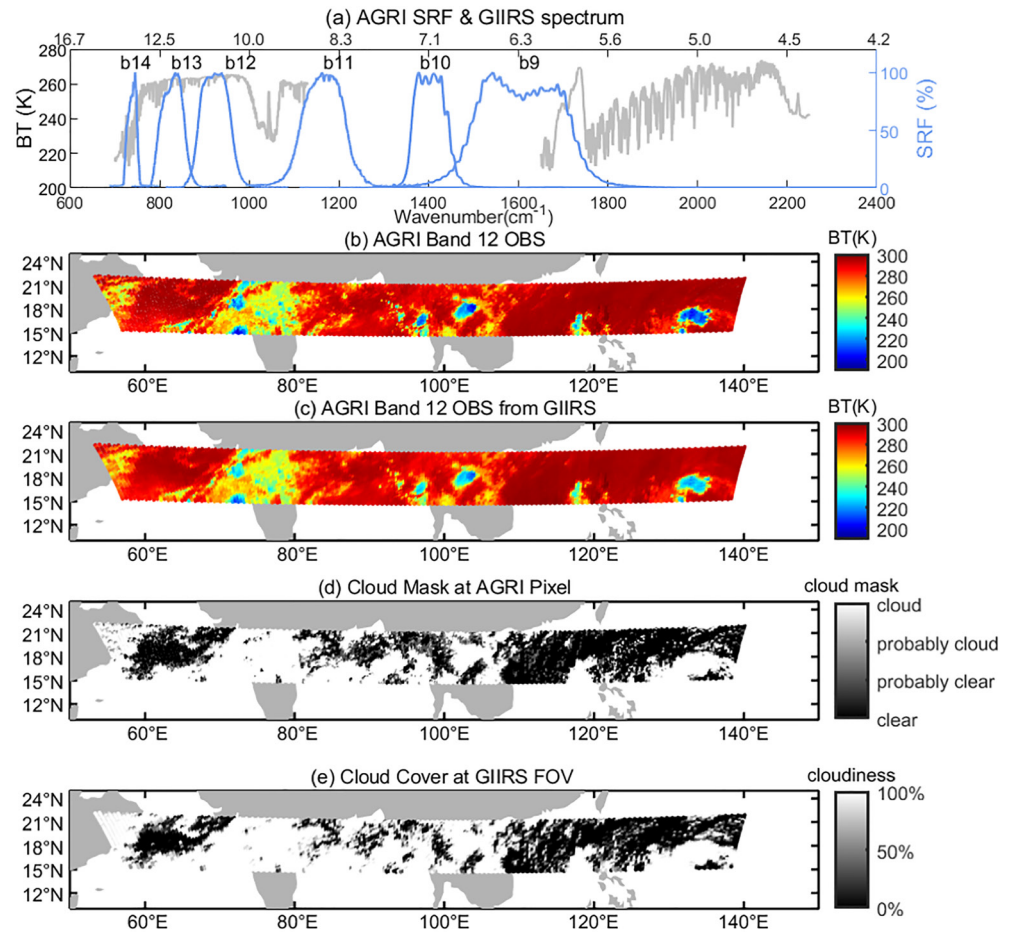


Figure 1. (a) Advanced Geosynchronous Radiation Imager (AGRI) IR bands 9–14 spectral response functions (blue) overlaying a geostationary interferometric infrared sounder (GIIRS) radiance spectrum (gray); (b) AGRI band 12 brightness temperature (BT) (K) at GIIRS field of views; (c) GIIRS convolved BTs for AGRI band 12; (d) BT differences between b and c; (e) Cloud mask at AGRI pixels; (f) GIIRS cloud coverage derived from AGRI cloud mask products. The time is 0000–0015 UTC on 01 June 2020.

this study, GIIRS Level 1B radiance observations from 01 to 07 July 2020, along with AGRI L1B, cloud mask, and CTH data are used.

2.2. Methodology

The basic premise for inter-calibration is that the two instruments view the same target at the same time with the same spectral region at the same viewing angle, which requires matching observations from the two sensors spatially, temporally, spectrally, and with the same viewing geometry. Once matched together, the radiances from all imager pixels within each sounder footprint are spatially averaged, while the hyperspectral IR radiances are spectrally convolved to the imager IR bands by applying the spectral response functions (SRFs). Figure 1a shows the SRFs of AGRI bands 8 – 14 overlaying a GIIRS radiance spectrum. In this image, the GIIRS longwave region almost fully covers AGRI bands 12, 13, and 14, and partly covers AGRI bands 9, and 11, while there is almost no spectral overlap between GIIRS and AGRI bands 10. Based on evaluation with forecasts from an NWP model (Liu et al., 2022; Yin et al., 2020), the calibration uncertainty is relatively larger around 750 cm⁻¹ for GIIRS/FY-4A. Therefore, only AGRI bands 12 (A12) and 13 (A13) are used for inter-calibration in this study; the GIIRS radiances are spectrally averaged to A12 and A13 using the following formula (Di et al., 2019):

$$\hat{rad} = \frac{\int_{\nu_1}^{\nu_2} rad(\nu) f(\nu) d\nu}{\int_{\nu_1}^{\nu_2} f(\nu) d\nu} \quad (1)$$

Where ν is the wavenumber, $f(\nu)$ is the corresponding AGRI band SRF; $rad(\nu)$ is the GIIRS radiance observation at channel ν , \hat{rad} is the convolved AGRI band radiance from GIIRS. Then BT is converted from \hat{rad} using the following formula:

$$BT = \left\{ \frac{c_2 * \nu_c}{\ln[1 + (c_1 * \nu_c^3) / \hat{rad}]} - bc_1 \right\} / bc_1 \quad (2)$$

where ν_c is the central wavenumber of AGRI band; c_1 and c_2 are the Planck function constants, $c_1 = 1.19104 \times 10^{-5}$ (mW/m²/sr/cm⁻⁴), $c_2 = 1.43877$ (K/cm⁻¹); bc_1 and bc_2 are the band correction coefficients, which are from the Radiative Transfer for TOVS coefficient file for the AGRI imagers.

The AGRI/FY-4A has two observation modes: (a) every 15 min for the full disk and (b) every 5 min for the China region. In contrast, GIIRS/FY-4A typically observes China and the adjacent regions every 2 hr. Based on these observation modes, AGRI and GIIRS observations are temporally matched with time differences of less than 15 min, while spatial matching uses Line-Of-Sight which is a fast and accurate method proposed by Wang et al. (2016).

To understand the scene dependence, the cloud coverage for each GIIRS footprint is calculated with a collocated AGRI cloud mask. Each AGRI pixel is classified as clear, probably clear, cloudy, and probably cloudy based on its cloud mask product. By counting the cloudy AGRI pixels within a GIIRS FOV, the cloud coverage at GIIRS FOV is inferred. The GIIRS footprint cloud coverage ranges from 0% (completely clear) to 100% (completely cloudy or overcast). Here, probably clear pixels and probably cloudy pixels are regarded as clear pixels and cloudy pixels, respectively. The CTH of the GIIRS footprint is also derived from the operational AGRI product (not shown in Figure 1). Figure 1 shows the mean AGRI band 12 BT observations at GIIRS FOVs, the AGRI band 12 BT spectrally convolved from GIIRS, and the corresponding BT differences, along with the AGRI cloud mask and GIIRS footprint cloud coverage derived from the AGRI cloud mask.

3. Results and Analysis

To avoid anomalous observations in the comparisons, a spatial uniform check is adapted to reject certain outliers on a statistical basis. In this study, scene uniformity is determined based on the surrounding environment, which is a box of 9×9 AGRI pixels centered at the collocated location, and the environment scene is considered homogeneous when the ratio of the AGRI BT standard deviation (STD) to the AGRI mean BT is less than 0.02 (He et al., 2022; Hu et al., 2013; Zhang & Gunshor, 2013). Choosing a uniform environment (9×9 AGRI pixels) rather than a GIIRS FOV (4×4 AGRI pixels) could make the comparison insensitive to a moving target (e.g., clouds) (He et al., 2022; Hewison et al., 2013).

The BIAS and the standard deviation (STD) of BTD are calculated using the following two equations:

$$BT D_i = BT_{agri} - BT_{giirs} \quad (3)$$

$$BIAS = \frac{1}{N} \sum_{i=1}^N BT D_i \quad (4)$$

$$STD = \frac{1}{N} \sqrt{\sum_{i=1}^N (BT D_i - BIAS)^2} \quad (5)$$

where BT_{agri} and BT_{giirs} represent the BT of AGRI spatially averaged at the GIIRS FOV and the spectrally convoluted BT (converted from convoluted radiance) of AGRI from GIIRS measurements. N is the sample size.

Please note that the results for band 13 are quite similar to band 12. Only the results for band 12 are listed in the paper.

3.1. Scene Radiance Dependence

Figures 2a–2c show the BIAS and STD for band 12 as a function of scene temperature under clear, partially cloudy, and overcast situations, respectively. Under clear skies, both BIAS and STD are relatively less scene/target

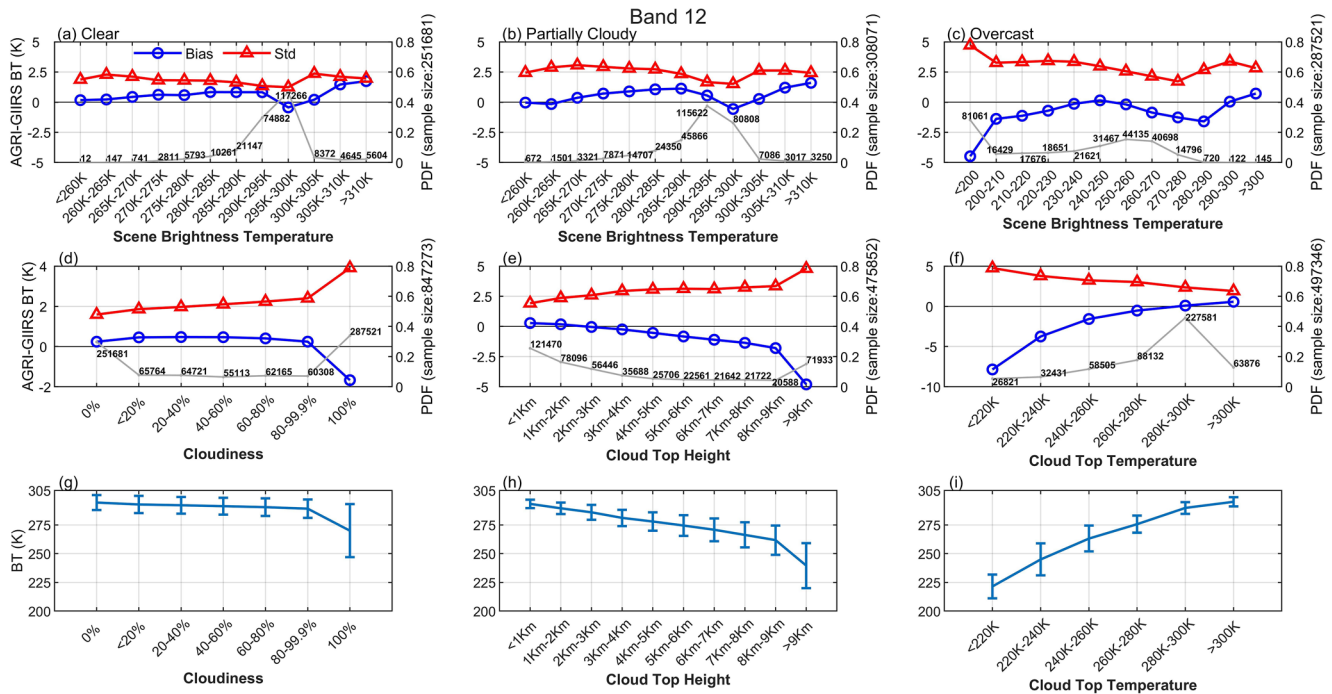


Figure 2. (a, b and c) BIAS and STD for band 12 as a function of scene brightness temperature (BT) under clear (left), partly cloudy (middle), and overcast (right) situations, respectively. (d, e and f) BIAS and STD for band 12 as a function of cloud coverage (left), cloud-top height (middle), and cloud-top temperature (right), respectively. g, h and i) Mean scene temperature at different scenes of cloud coverage (left), cloud-top height (middle) and cloud-top temperature (right), respectively. The geostationery interferometric infrared sounder measurements are used as scene BT in the first and third row of figures. Data is from 01–07 July 2020.

temperature dependent. However, under cloudy situations, especially those that are overcast, the scene temperature dependence is significant; for example, when the scene becomes colder, the BIAS and STD are larger. The large cold biases of the IR window bands at low-temperature scenes were also similarly presented in the inter-comparisons of LEO broad band imagers (e.g., VIIRS, MODIS) and hyperspectral sounder measurements (Gong et al., 2018; Moeller et al., 2013; Veglio et al., 2016). And it is interesting to see that the bias reaches a local minima of around 295–300K under a clear and partially cloudy situation, which presumably is close to the temperature of the black body.

3.2. Cloud Scene Dependence

Figures 2d, 2e and 2f show the variation in BIAS and STD as a function of cloudiness, CTH, and cloud-top temperature (CTT), respectively. As seen in the figure, BIAS and STD are only weakly sensitive to the cloudiness/cloud cover within the footprint, except when the cloudiness is near overcast (from 99.9% to 100%). However, they are relatively sensitive to CTH/CTT. Combined with Figures 3g–3i showing the mean scene BTs for different cloudy situations, BIAS and STD are more influenced by scene temperature than the presence of clouds within the footprint. To be more specific, for AGRI, the calibration uncertainty is more relevant to the temperature of scene, and the inconsistency between AGRI and GIIRS BT observations is more noticeable in low temperature scenes (e.g., overcast, high cloud situation). The relatively larger calibration uncertainty in low temperature scenes could be partly attributed to the fact that the nonlinearity of the Planck function for cooler BTs is more significant than for warmer BTs when converting the radiance to BT (Berk, 2008; DeSlover, 1996; Di et al., 2019; Weinreb et al., 1981). Since the GIIRS radiances are spectrally averaged to GIIRS bands by linearly applying SRFs, the nonlinearity might cause uncertainty in the inter-comparisons when the scene is cold. For further investigation, the variation in BIAS and STD as a function of cloudiness, CTH and CTT after correcting for the radiance dependence is given in the Supplemental document (Figure S2 of Supporting Information S1), and which clearly shows that the BIAS is almost insensitive to the cloudiness, CTH or CTT. In addition, the bias in the radiance (Figure S1 of Supporting Information S1) increases a little bit slower as the scene becomes colder than the bias in the radiance, so the nonlinearity of the Planck function contributes to the obvious bias changing for cold scenes.

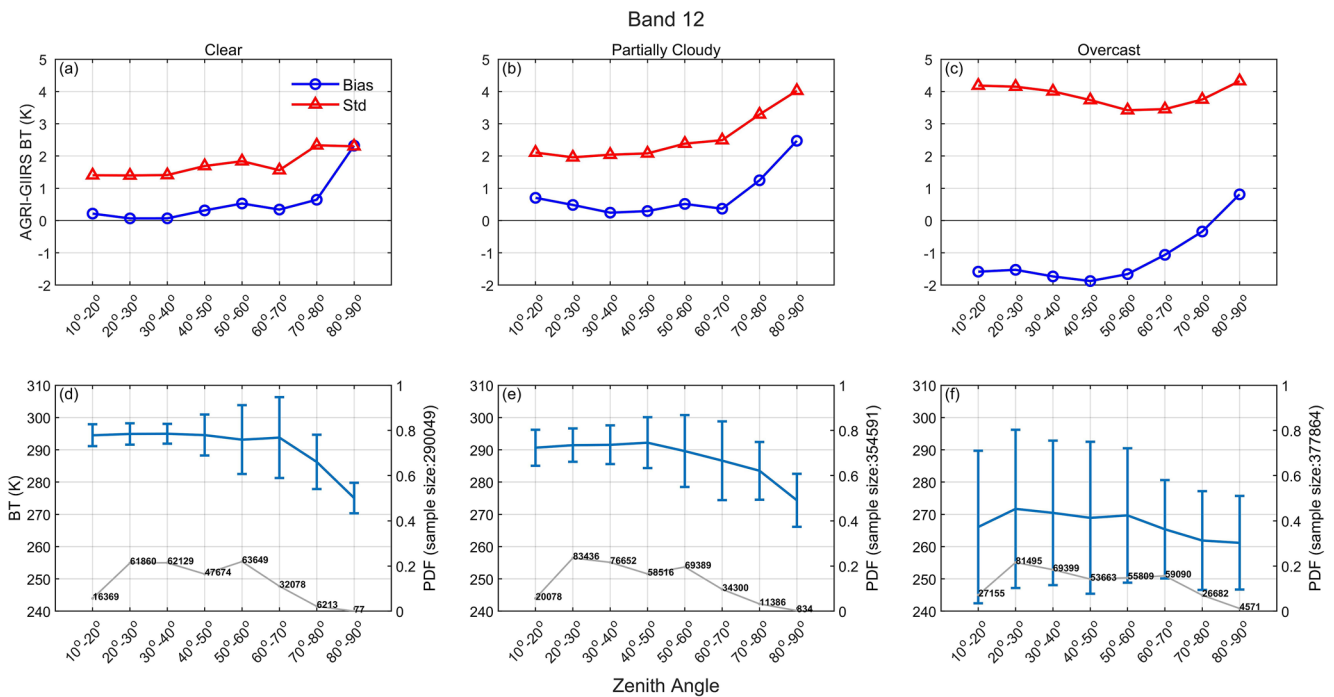


Figure 3. a, b, and (c) BIAS and STD of Advanced Geosynchronous Radiation Imager bands 12 (upper) as function of local zenith angle under clear (left), partially cloudy (middle), and overcast (right) scenes, respectively. (d, e and f) Mean scene temperature with different local zenith angles under clear (left), partially cloudy (middle), and overcast (right) scenes.

3.3. Angle Dependence

Figure 3 shows the AGRI band 12 BIAS and STD between AGRI and GIIRS (AGRI-GIIRS) as a function of local zenith angle (LZA), under clear, partially cloudy, and overcast scenes, respectively. The BIAS and STD are relatively stable for the two bands when the LZA is less than 70° under clear and partially cloudy situations. However, when the LZA is greater than 70°, both BIAS and STD increase with angle, while under overcast skies, the BIAS increases much faster when the LZA is larger than 60°. In addition, under overcast situations, the BIAS and STD are significantly larger, which might be due to the colder scene in overcast situations. The BIAS is positive under clear and partly cloudy skies, which indicates a warm bias usually less than 0.5 K for bands 12 and 13, respectively, when the LZA is less than 70°. As a result, products such as sea surface temperature, surface skin temperature, and surface emissivity, etc., could be impacted. The BIAS is negative under overcast situations, which indicates a cold bias usually between -1 and -2 K when the LZA is less than 70°. This significant cold bias should be further understood since it could impact the quality of cloud-top products such as cloud-top height and cloud phase. It should be noted that the samples are small when the LZA is greater than 70° so the statistical significance is less than for those with an LZA less than 70°. As shown in Figure 3 when the scene temperature decreases quickly when the LZA is over 60°, the angle dependence might come from the scene temperature dependence; while after the correction in the radiance dependence (see Figure S3 of Supporting Information S1), it still exhibits an obvious angle dependency—BIAS and STD still increase quickly when the LZA is over 60–70°, although the bias is smaller with the correction.

According to these results, in addition to the scene uniformity, the LZA check is noteworthy and necessary. To better understand the diurnal characteristics of BT, strict quality control with LZA values less than 60° for both bands is used for further comparisons and analysis in the following sections.

3.4. Diurnal Variation of BT Differences

Figure 4 shows the BIAS and STD as a function of time under clear, partly cloudy, and overcast situations, as well as over land and ocean. The results reflect the diurnal characteristics of BIAS and STD. It should be noted that due to a lack of observations between 1600 and 1800 UTC (the GIIRS sensor does not operate during this

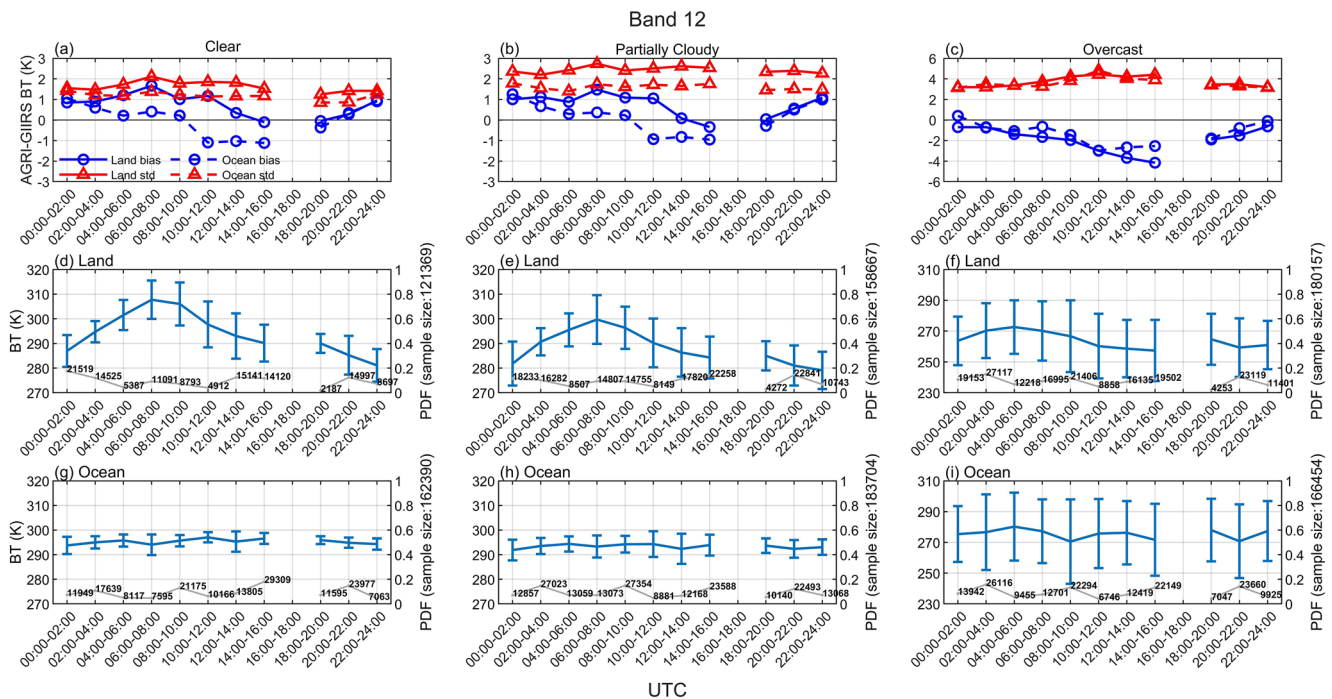


Figure 4. a, b and c) BIAS and STD as a function of time under clear (left), partly cloudy (middle), and cloudy situation (right), respectively, over land (solid) and ocean (dash); d, e and f) the mean geostationery interferometric infrared sounder (GIIRS) brightness temperature (BTs) and sample sizes as a function of time over land; g, h and i) show the mean GIIRS BTs and sample sizes as a function of time over ocean.

period), there is a gap in observation continuity. Overland, significant diurnal variation is observed in the BIAS. Between 0000–0800 UTC and 1800–2400 UTC (Beijing local time 08:00–16:00 and the next day 02:00–08:00), the BIAS increases, while between 0800 and 1600 UTC (Beijing local time 16:00–02:00 of the next day), the BIAS decreases over land under clear skies and partly cloudy skies. In contrast, the diurnal variation in STD is relatively small, less than 0.5 K in magnitude under clear skies and partly cloudy skies, while the STD varies over 2K under overcast situations. Over the ocean, the BIAS and STD are relatively smaller under clear skies and partly cloudy skies and the diurnal variation in BIAS is not the same as that over the land. It is likely due to smaller BT variations over the ocean (the sea surface temperature is more stable than the land surface temperature). Under overcast situations, the diurnal variation in BIAS over land and ocean is much closer but differs from that under partly cloudy skies and clear skies. As discussed above, the relatively low calibration accuracy for cooler BTs might contribute to this phenomenon. Overall, the BIAS is within 2 K under clear and partly cloudy skies, and the STD is also within a reasonable range. The BT consistencies between GIIRS and AGRI are higher over the ocean than over land. After the correction for radiance-dependency (please see Figure S4 in the supplemental document), the magnitudes of the diurnal variation in bias under clear, partly cloudy, and cloudy situations almost decrease 1K, but they still exhibit obvious diurnal variation patterns.

The diurnal variation in BIAS can easily be determined when a hyperspectral IR sounder is onboard the same GEO platform, while it also can be achieved by comparing with IR sounders on multiple LEO platforms with different equator crossing times. The diurnal variation in bias could impact products and applications; for example, the CTH during severe storm development (e.g., Typhoon) could be overestimated or underestimated.

4. Summary and Discussion

When the hyperspectral IR sounder and imager are on the same GEO platform, the GEO imager IR bands can be inter-calibrated with much larger spatial coverage with different scenes. This method allows for better analysis and understanding of the spatial and temporal characteristics of the BIASs between the imager and sounder, which benefits product assurance and data assimilation applications. Using GIIRS and AGRI from FengYun-4A, the first satellite of the FengYun-4 series, this study addresses GEO imager specific calibration questions such as viewing angle dependence, scene (clouds, etc.), and diurnal characteristics.

Based on the comparison of collocated AGRI band 12 and band 13 with GIIRS measurements from 01 to 07 July 2020, it is found that.

1. the BT inconsistencies are less scene/target temperature dependent under clear and partially cloudy situations, while under overcast cloudy situations, the scene temperature dependence is significant. The imager calibration uncertainty is more relevant to the temperature of the scene, and the BT inconsistency between AGRI and GIIRS is more noticeable in low temperature scenes (e.g., overcast, high cloud situations).
2. the BT inconsistencies are less dependent on the angle when the LZA is less than 70° under both clear and partially cloudy situations. While under completely cloudy or overcast situations, BT inconsistencies increase significantly when the LZA is over 60°.
3. Significant BIAS diurnal characteristics and relatively stable STD under clear and partially cloudy situations are found; even larger diurnal variations in BIAS and STD under overcast situations are revealed.

Understanding the characteristics of calibration bias and uncertainty is not only important to improving satellite products such as cloud-top phase, cloud-top temperature, sea surface temperature, surface skin temperature, surface emissivity, etc., derived from imager radiance observations for applications, but also it is important to the synergistic use of imager and sounder data when both sensors are onboard the same platform. For example, using an optimal cloud-clearing methodology (Li et al., 2005), cloud-cleared radiances are greatly enhanced for assimilating into NWP models by using imager data within the sounder sub-footprint (Wang et al., 2017). Applying the optimal cloud-clearing method requires small radiance differences between imager observations spatially averaged to the sounder footprint and sounder observations spectrally averaged to the imager bands; such radiance differences can also be used to develop quality flags for cloud-cleared radiances. This study shows comparable accuracy of IR measurements under partially cloudy situations when compared with the measurements from clear skies. Therefore, the methodology and analysis can be used together with an optimal cloud-clearing process to produce GIIRS cloud-cleared radiances with good quality when combined with AGRI for applications such as data assimilation (Li et al., 2021).

Data Availability Statement

All the data used in the study including GIIRS radiance measurements, AGRI radiance measurements, and cloud relevant products could be downloaded from <http://satellite.nsmc.org.cn/PortalSite/Data/Satellite.aspx?currentculture=zh-CN>. Please note that data is available after registration.

References

- Aumann, H. H., Broberg, S., Elliott, D., Gaiser, S., & Gregorich, D. (2006). Three years of Atmospheric Infrared Sounder radiometric calibration validation using sea surface temperatures. *Journal of Geophysical Research*, 111(D16), D16S90. <https://doi.org/10.1029/2005jd006822>
- Berk, A. (2008). Analytically derived conversion of spectral band radiance to brightness temperature. *Journal of Quantitative Spectroscopy & Radiative Transfer*, 109(7), 1266–1276. <https://doi.org/10.1016/j.jqsrt.2007.09.016>
- Bessho, K., Date, K., Hayashi, M., Ikeda, A., Imai, T., Inoue, H., et al. (2016). An introduction to Himawari-8/9—Japan's new-generation geostationary meteorological satellites. *Journal of the Meteorological Society of Japan. Ser. II*, 94(2), 151–183. <https://doi.org/10.2151/jmsj.2016-009>
- Blumstein, D., Tournier, B., Cayla, F. R., Phulpin, T., Fjortoft, R., Buil, C., & Ponce, G. (2007). In-flight performance of the infrared atmospheric sounding Interferometer (IASI) on METOP-A. In *Atmospheric and Environmental Remote Sensing Data Processing and Utilization III: Readiness for GEOSS* (Vol. 6684, pp. 103–114). SPIE.
- DeSlover, D. H. (1996). *Analysis of visible and infrared cirrus cloud optical properties using high spectral resolution remote sensing*. University of Wisconsin--Madison.
- Di, D., Min, M., Li, J., & Gunshor, M. M. (2019). The radiance differences between wavelength and wavenumber spaces in convolving hyperspectral infrared sounder spectrum to broadband for intercomparison. *Remote Sensing*, 11(10), 1177. <https://doi.org/10.3390/rs11101177>
- Gong, X., Li, Z., Li, J., Moeller, C. C., Cao, C., Wang, W., & Menzel, W. P. (2018). Intercomparison between VIIRS and CrIS by Taking into Account the CrIS Subpixel cloudiness and viewing geometry. *Journal of Geophysical Research: Atmospheres*, 123(10), 5335–5345. <https://doi.org/10.1029/2017JD027849>
- Guo, Q., Yang, J., Wei, C., Chen, B., Wang, X., Han, C., et al. (2021). Spectrum calibration of the first hyperspectral infrared measurements from a geostationary platform: Method and preliminary assessment. *Quarterly Journal of the Royal Meteorological Society*, 147(736), 1562–1583. <https://doi.org/10.1002/qj.3981>
- He, X., Xu, N., Feng, X., Hu, X., Xu, H., & Peng, Y. (2022). Assessing radiometric calibration of FY-4A/AGRI thermal infrared channels using CrIS and IASI. *IEEE Transactions on Geoscience and Remote Sensing*, 60, 1–12. <https://doi.org/10.1109/TGRS.2021.3111975>
- Hewison, T. J., Wu, X., Yu, F., Tahara, Y., Hu, X., Kim, D., & Koenig, M. (2013). GSICS inter-calibration of infrared channels of geostationary imagers using Metop/IASI. *IEEE Transactions on Geoscience and Remote Sensing*, 51(3), 1160–1170. <https://doi.org/10.1109/TGRS.2013.2238544>
- Hu, X., Xu, N., Weng, F., Zhang, Y., Chen, L., & Zhang, P. (2013). Long-term monitoring and correction of FY-2 infrared channel calibration using AIRS and IASI. *IEEE Transactions on Geoscience and Remote Sensing*, 51(10), 5008–5018. <https://doi.org/10.1109/tgrs.2013.2275871>

Acknowledgments

This study is supported by the Chinese National Natural Science Foundation 42105126 (Di Di), U2142201 (Jun Li), and 41905098 (Xinya Gong). CMA is thanked for providing the GIIRS radiance measurements, AGRI radiance measurements, and cloud mask products. All the data used in the study could be downloaded from <http://satellite.nsmc.org.cn/PortalSite/Data/Satellite.aspx?currentculture=zh-CN>.

- Li, J., Liu, C. Y., Huang, H. L., Schmit, T. J., Wu, X., Menzel, W. P., & Gurka, J. J. (2005). Optimal cloud-clearing for AIRS radiances using MODIS. *IEEE Transactions on Geoscience and Remote Sensing*, 43(6), 1266–1278. <https://doi.org/10.1109/tgrs.2005.847795>
- Li, J., Okamoto, K., Geer, A., Otkin, J., Liu, Z., Han, W., & Wang, P. (2021). Satellite all-sky infrared radiance assimilation: Recent progress and future perspectives. *Advances in Atmospheric Sciences*, 39(1), 9–21. <https://doi.org/10.1007/s00376-021-1088-9>
- Liu, J., Xu, L., Cheng, W., Wang, B., Gong, X., Deng, Z., et al. (2022). Bias characteristics and bias correction of GHIRS on board FY-4A for data assimilation. *Chinese Journal of Atmospheric Sciences*. <https://doi.org/10.3878/j.issn.1006-9895.2000.19000>
- Menzel, W. P., Schmit, T. J., Zhang, P., & Li, J. (2018). Satellite-based atmospheric infrared sounder development and applications. *Bulletin of the American Meteorological Society*, 99(3), 583–603. <https://doi.org/10.1175/bams-d-16-0293.1>
- Moeller, C., Tobin, D., & Quinn, G. (2013). S-NPP VIIRS thermal band spectral radiance performance through 18 months of operation on-orbit. *Proceedings of SPIE*, 8866, 88661N. <https://doi.org/10.1117/12.2023389>
- Schmit, T. J., Gunshor, M. M., Menzel, W. P., Gurka, J. J., Li, J., & Bachmeier, A. S. (2005). Introducing the next-generation advanced baseline imager on GOES-R. *Bulletin of the American Meteorological Society*, 86(8), 1079–1096. <https://doi.org/10.1175/bams-86-8-1079>
- Taylor, J. K., Tobin, D. C., Revercomb, H. E., Best, F. A., Garcia, R. K., Motteler, H., & Goldberg, M. (2015). Suomi NPP/JPSS cross-track infrared sounder (CrIS): Calibration validation with the aircraft based scanning high-resolution interferometer sounder (S-HIS). In *Fourier Transform Spectroscopy* (p. FW1A-3). Optica Publishing Group.
- Veglio, P., Tobin, D. C., Dutcher, S., Quinn, G., & Moeller, C. C. (2016). Long-term assessment of Aqua MODIS radiance observation using comparisons with AIRS and IASI: AIRS-MODIS long-term comparison. *Journal of Geophysical Research: Atmospheres*, 121(14), 8460–8471. <https://doi.org/10.1002/2015JD024653>
- Wang, L., Cao, C., & Goldberg, M. (2009). Intercalibration of GOES-11 and GOES-12 water vapor channels with MetOp IASI hyperspectral measurements. *Journal of Atmospheric and Oceanic Technology*, 26(9), 1843–1855. <https://doi.org/10.1175/2009jtecha1233.1>
- Wang, L., Goldberg, M., Wu, X., Cao, C., Iacovazzi, R. A., Yu, F., & Li, Y. (2011). Consistency assessment of atmospheric infrared sounder and infrared atmospheric sounding interferometer radiances: Double differences versus simultaneous nadir overpasses. *Journal of Geophysical Research*, 116(D11), D11111. <https://doi.org/10.1029/2010JD014988>
- Wang, L., Tremblay, D., Zhang, B., & Han, Y. (2016). Fast and accurate collocation of the visible infrared imaging radiometer suite measurements with cross-track infrared sounder. *Remote Sensing*, 8(1), 76. <https://doi.org/10.3390/rs8010076>
- Wang, P., Li, J., Li, Z., Lim, A. H., Li, J., Schmit, T. J., & Goldberg, M. D. (2017). The impact of cross-track infrared sounder (CrIS) cloud-cleared radiances on Hurricane Joaquin (2015) and Matthew (2016) forecasts. *Journal of Geophysical Research: Atmospheres*, 122(24), 13201–13218. <https://doi.org/10.1002/2017jd027515>
- Weinreb, M. P., McMillin, L. M., Fleming, H. E., & Neuendorffer, A. C. (1981). Transmittances for the TIROS operational vertical sounder.
- Wu, X., Hewison, T., & Tahara, Y. (2009). GSICS GEO-LEO intercalibration: Baseline algorithm and early results. In *Atmospheric and Environmental Remote Sensing Data Processing and Utilization V: Readiness for GEOSS III* (Vol. 7456, pp. 25–36). SPIE.
- Yang, J., Zhang, Z., Wei, C., Lu, F., & Guo, Q. (2017). Introducing the new generation of Chinese geostationary weather satellites, Fengyun-4. *Bulletin of the American Meteorological Society*, 98(8), 1637–1658. <https://doi.org/10.1175/bams-d-16-0065.1>
- Yin, R., Han, W., Gao, Z., & Di, D. (2020). The evaluation of FY4A's Geostationary Interferometric Infrared Sounder (GHIRS) long-wave temperature sounding channels using the GRAPES global 4D-Var. *Quarterly Journal of the Royal Meteorological Society*, 146(728), 1459–1476. <https://doi.org/10.1002/qj.3746>
- Zhang, Y., & Gunshor, M. M. (2013). Intercalibration of FY-2C/D/E infrared channels using AIRS. *IEEE Transactions on Geoscience and Remote Sensing*, 51(3), 1231–1244. <https://doi.org/10.1109/tgrs.2013.2242897>